Inferno Worlds

Ridden - Harper, A.

4 Self-shielding in dust tails of disintegrating rocky exoplanets

Context. Chapter 3 presents a new 3D model to simulate the dust-tails and transit light curves of disintegrating rocky exoplanets. The model combines a code to calculate the dynamics of dust particles and a radiative transfer code (MCMax3D) to produce transit light curves for the simulated tails. While the model correctly treats opacity both in the optically thick and thin regimes for the light curve calculations, the radiation pressure is calculated correctly only in the optically thin case. The model therefore neglects self-shielding which can affect the dust particle dynamics and the resulting tail morphology.
Aims. To make the model fully self-consistent, we aim to incorporate self-shielding and investigate how it affects the morphology and transit light curves of dust tails from disintegrating rocky exoplanets.
Methods. We extend the model to account for self-shielding in the dynamics of dust-particles by calculating optical depths to each particle on a spherical 3D grid using the Planck mean opacity. Shielded particles receive a reduced stellar flux, which decreases both the radiation pressure and the sublimation rate that they experience.
Results. We show that, self-shielding can have a strong influence on the dynamics and morphology of dust tails and their corresponding transit light curves. In the particular case of Kepler-1520 b, the average transit depth can be reproduced with a mass-loss rate of $3 - 3.9\ M_\oplus\ Gyr^{-1}$, which is lower than the value derived in Chapter 3 for non-self-shielding tails because the particles do not sublimate as quickly. However, this reduced sublimation rate makes it more likely that particles survive for more than one orbit, violating the observed lack of correlation between transits (van Werkhoven et al. 2014), except if the composition of the dust particles is such that they have a particularly high sublimation rate. We also show that the outbursts of mass-loss can be much shorter than an orbital period and that mass-loss rates $\gtrsim 10\ M_\oplus\ Gyr^{-1}$ only produce long tails if they are continuous for several orbits due to the strong self-shielding slowing the drift rate of particles away from the planet. Such tails produce correlated increasing transit depths, providing an observational signature that may be exploited in the era of TESS.

4.1 Introduction

The Kepler Space Telescope has revealed a class of small, short-period rocky exoplanets that have a 'comet-like' dust tail that produces variable and asymmetric transit light curves of which Kepler 1520 b (formerly known as KIC 12557548 b) is the archetype (Rappaport et al. 2012, 2014; Sanchis-Ojeda et al. 2015; Vanderburg et al. 2015). Studying the properties of this dust provides unique insights into the composition of the parent planet. By fitting the average transit shape with dust tail models, including brightening from forward scattering, parameters such as the particle size, particle composition and mass-loss rate have been constrained (Rappaport et al. 2012, 2014; Brogi et al. 2012; Budaj 2013; van Lieshout et al. 2014; Sanchis-Ojeda et al. 2015; van Lieshout et al. 2016), which can be further investigated using spectroscopic transit observations (e.g. Croll et al. 2014; Murgas 2013; Bochinski et al. 2015; Alonso et al. 2016).

Since a large amount of dust is released from a small planet, the dust is bound to be optically thick close to the planet. Previous modeling efforts confirm this (van Lieshout et al. 2016). We therefore embarked on an effort to develop a new model that simulates optically thick dust tails for the first time. A two-step approach was implemented in our earlier model (Chapter 3). First, a dust tail was built up by ejecting particles in 3D from the surface of a planet to calculate their subsequent dynamics under the influence of the star's radiation pressure and the planet's gravity assuming optically thin conditions. Subsequently, the 3D dust-mass distribution in the tail was gradually scaled up to make them partially or completely optically thick. Using this model, it was found that increasing the optical depth of a dust tail makes the transit depth more achromatic, and a constraint was derived on the particle ejection velocity for a given planet mass under the assumption that the particles are not accelerated by gas after they leave the planet. In Chapter 3, planet mass-loss rates for Kepler-1520 b were derived which are $10-100$ times higher than those inferred by previous studies that used fully optically thin tail models. This is due to the fact that optically thick tails allow some mass to be 'hidden', which does not contribute to the transit depth.

The approach taken in Chapter 3 is, however, not completely self-consistent. In the case that a dust tail is (partially) optically thick, some fraction of the dust particles will be shielded from stellar radiation, slowing down their sublimation and decreasing the radiation pressure. This may affect the overall morphology (length and shape) of the dust tail. This motivates the work presented here, which extends the model in Chapter 3 to account for self-shielding when simulating the dust particle dynamics and evolution for the first time. We note that self-shielding of gas only has been implemented in a model by Bourrier et al. (2014) for a different astrophysical phenomenon, the comet-like gas-tails resulting from atmospheric escape of the hot Jupiters HD 209458 b and HD 189733 b.

This chapter is structured as follows: Section 4.2 explains the model, Section 4.3 presents and discusses the results of the simulations and Section 4.4 concludes.

4.2 Method: The model

The original model that forms the basis of this study was fully described in Chapter 3. In brief, it builds up a dust tail by ejecting meta-particles, which individually represent a large number of dust particles, from the surface of a small rocky exoplanet. After the meta-particles are ejected, they move under the influence of the planet's gravitational force, the stellar radiation pressure, and the stellar gravitational force. The ratio of the latter two forces, β, is independent of the distance from the star, and only depends on the stellar luminosity and the dust scattering properties, which are set by the particle composition, radius and shape (e.g. Burns et al. 1979).

Values of β were computed as in van Lieshout et al. (2014) by assuming a composition of corundum (Al_2O_3). This was found by van Lieshout et al. (2016) to be consistent with the observations, although other compositions such as iron-rich silicates are also possible. Our meta-particles become smaller with time due to sublimation, so we allow the value of β to change consistently with the change in particle radius. Transit light curves are subsequently generated for these simulated tails by using the radiative transfer code MCMax3D[1] (Min et al. 2009) which calculates the wavelength-dependent light curves for optically thick dust tails.

In the original study of Chapter 3, dust particle dynamics were calculated using an optically thin approximation, meaning that each particle receives the full amount of radiation pressure. Total opacity calculations, including those in the optically thick regime, were achieved by scaling up the mass distribution only after the particle dynamics were determined. However, this is not a fully self-consistent approach, since optical depth effects can shield parts of the dust particle ensemble from stellar radiation. This self-shielding influences both the sublimation rate and the particle trajectories, and is included in the model presented here.

All of our self-shielding simulations use the input parameters shown in Table 3.1, with option #2 for the planet mass and radius. However, optical depths are calculated on a higher resolution grid, defined by the cell boundaries given in Table 4.1. As with Chapter 3, these boundaries were set such that the planet is located on an intersection of grid lines so that particles released from different sides of the planet fall into different grid cells. The optical depth was calculated for each grid

[1] `http://www.michielmin.nl/codes/mcmax3D/`

position according to

$$\tau(r,\theta,\phi) = A\sum_{r=0}^{R}\sum_{a=a_{min}}^{a_{max}} \kappa(a)\rho(r,\theta,\phi,a)dr(\theta) \tag{4.1}$$

where a is the particle radius, r is the radial distance from the star, θ is the elevation angle relative to the orbital plane, ϕ is the azimuthal angle, $\kappa(a)$ is the particle size dependent Planck mean opacity[2], $\rho(r,\theta,\phi,a)$ is the mass density within a particular size bin, $dr(\theta)$ is the radial extent of the cell, which varies as a function of elevation relative to the planet's orbital plane, and A is the scaling factor to normalize the optical depths to those of MCMax3D. This was determined by comparing the optical depths calculated for our tail dynamics by those of MCMax3D. In the simulations for Kepler-1520 b, we set the $\kappa(a)$ dependence as for corundum particles in the appropriate radiation field set by the effective temperature of the host star. The optical properties of corundum were taken from Koike et al. (1995). The opacities were constructed assuming irregularly shaped particles computed using the distribution of hollow spheres (DHS) method from Min et al. (2005).

Subsequently, for each 3D grid position, the fractional flux $\mathfrak{F}$ that is transmitted through the radial column in the tail equals $e^{-\tau(r)}$ (ignoring the scattered flux field). This allows β to be modified to

$$\beta' = \mathfrak{F}\frac{F_{rad\ star}}{F_{grav\ star}} = \mathfrak{F}\beta. \tag{4.2}$$

We also account for the attenuated flux driving a reduced meta-particle sublimation rate, $\dot{a}'$, according to

$$\dot{a}' = \mathfrak{F}\dot{a} \tag{4.3}$$

where $\dot{a}$ is the assumed particle sublimation rate (change in radius per second) for particles that receive the unattenuated stellar flux.

As in Chapter 3, a value of $\dot{a}$ is assumed such that an unshielded particle that is ejected with a radius of 1 μm will have completely sublimated after exactly one orbital period. This is only a first-order approximation because in reality, the particle sublimation rate will depend on the particle size and temperature. However, for this work our focus was on investigating a general, optically thick tail, so our only requirements on sublimation rate were that it produced a tail of reasonable length and that unshielded meta-particles did not survive for longer than one orbit (since there is no correlation between consecutive transit depths (van Werkhoven et al. 2014)), making our simple approximation reasonable. The model was implemented as in Section 3.2.1, except that β' replaced β in Equation 3.1.

[2]The mean opacity, weighted according to the host stars's normalized Planck black body radiation energy density distribution.

Table 4.1: Radiative transfer grid parameters for the self-shielding simulations.

Parameter	Value
Radial grid	
Inner radius	0.0130 au
Outer radius	0.0152 au
Bin size	1.65×10^{6}
Elevation grid ($0^\circ - 180^\circ$)	
Lower elevation	89.58° (1)
Upper elevation	90.42° (2)
Bin size	0.0105°
Azimuthal grid ($0^\circ - 360^\circ$)	
Bin size	0.5°

(1) With an additional large bin containing $0^\circ - 89.58^\circ$.
(2) With an additional large bin containing $90.42^\circ - 180^\circ$.

For a completely optically thin tail, self-shielding should have a negligible effect on the particle dynamics and tail morphology. To confirm that this was indeed the case with our new model, we compared tails that were simulated both with and without self-shielding at different mass-loss rates. For these simulations we chose to eject meta-particles with an initial radius of 1 μm in a continuous and spherically symmetric distribution with a velocity of 3.13 km s^{-1} (1.03 times the surface escape velocity) from a planet of mass 0.02 M$_\oplus$. We assumed a planet bulk density equal to that of Mercury (5427 kg m^{-3}), giving a radius of 0.28 R$_\oplus$. We found that accounting for self-shielding produced no significant effect in the tail for mass-loss rates $\lesssim$0.1 M$_\oplus$ Gyr^{-1}, as shown by the first column of Fig. 4.2.

4.3 Results and Discussion

4.3.1 General effects of self-shielding

To investigate the effect of self-shielding on tail morphology and transit shape and depth, over a large mass-loss range, we first simulated self-shielding and non-self-shielding tails integrating the mass-loss over one orbital period of Kepler-1520 b. The transit depths are shown in the upper panel of Fig. 4.1, with their ratio shown in the lower panel. At mass-loss rates $<$1 M$_\oplus$ Gyr^{-1} both models show very similar depths due to the insignificant amount of self shielding. In the range $1 - 10$ M$_\oplus$ Gyr^{-1} the self-shielding models give a $20 - 40$% larger transit depth.

For mass-loss rates $\gtrsim$10 M$_\oplus$ Gyr^{-1} the self-shielding models give shallower transit depths (after one orbit). This behaviour is caused by self-shielding affecting

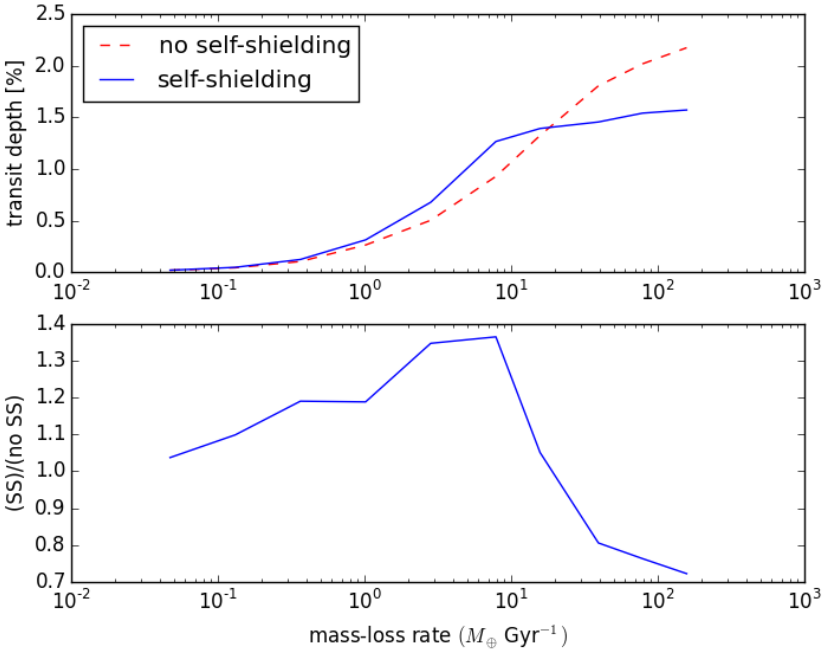

Figure 4.1: Top: Simulated transit depths from self-shielding (solid blue) and non-self-shielding (red dashed) tails after one orbit as a function of planet mass-loss rate. Bottom: Ratio of self-shielding to non-self-shielding transit depths after one orbit.

the transit depth in two opposing ways: #1) It reduces the particle sublimation rate so that more mass is retained in the tail, leading to deeper transit depths. #2) It reduces the radiation pressure, slowing the drift rate of particles away from the planet. This increases the time required for a long tail to form so that after one orbit, there is a smaller transit-cross section compared to the non-self-shielding case, leading to shallower transit depths. In the mass-loss rate range of $1 - 10$ M$_\oplus$ Gyr^{-1}, the moderate self-shielding causes reason #1 to dominate while for mass-loss rates $\gtrsim$10 M$_\oplus$ Gyr^{-1}, the stronger self-shielding cases reason #2 to dominate. The long-term evolution of self-shielded tails is discussed in Section 4.3.5.

The effect of self-shielding on tail morphology is illustrated in Fig. 4.2 for mass-loss rates of 0.1, 1, 10, and 100 M$_\oplus$ Gyr^{-1}. The top-row panels show the X-Y view (from above the orbital plane), the middle-row panels show the X-Z view (in the orbital plane), and the bottom row shows the transit light curves.

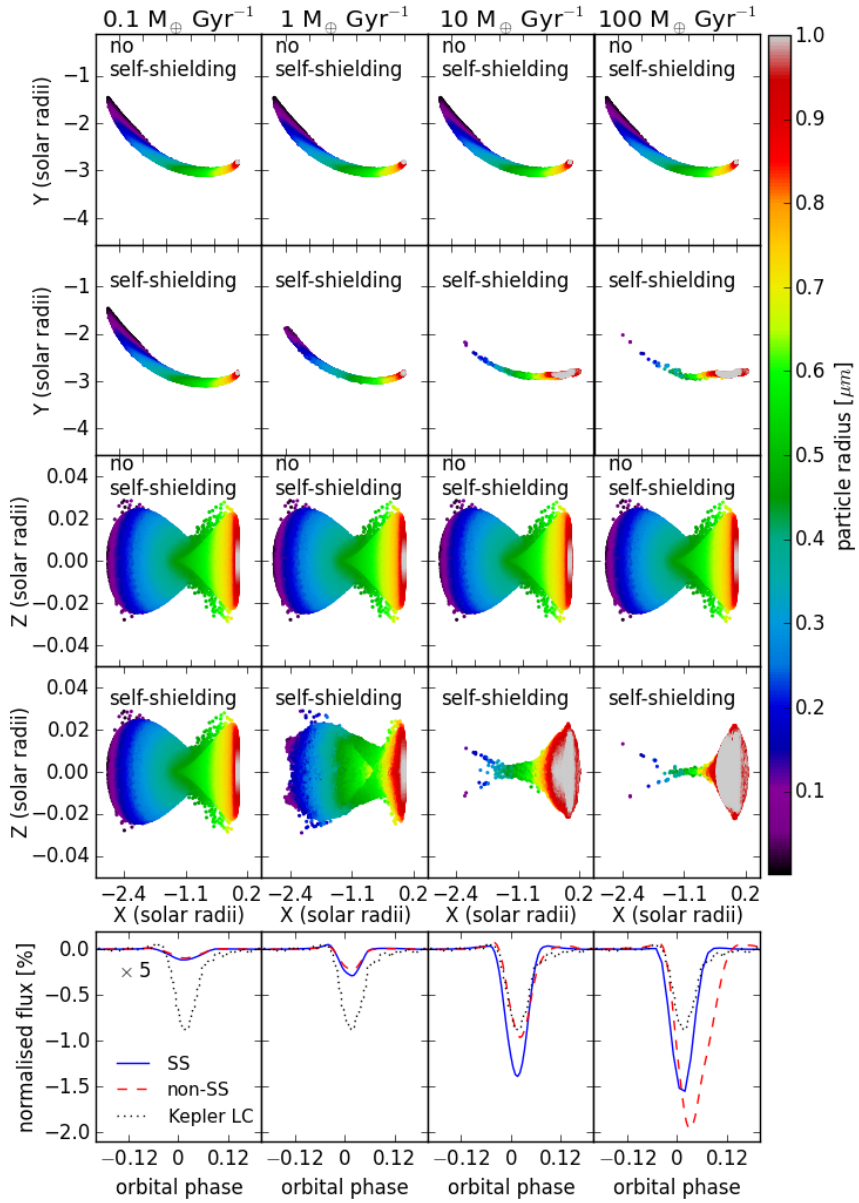

Figure 4.2: Simulated dust tails and their transit light curves after evolving over one orbit of Kepler-1520 b with and without accounting for self-shielding, for mass-loss rates of 0.1, 1, 10 and 100 $M_\oplus$ Gyr^{-1}. The 3D tails are viewed from above the orbital plane (first two rows) and along the orbital plane (second two rows). The simulated light curves were convolved with the Kepler long cadence exposure window function and the transit depths for the 0.1 $M_\oplus$ Gyr^{-1} case were increased by a factor of 5 for clarity.

4.3.2 Fitting the average transit of Kepler-1520 b with the self-shielding model

Since accounting for self-shielding reduces the effective sublimation rate, the average transit depth of Kepler-1520 b can be produced with a lower mass-loss rate than was required in Chapter 3. To determine the required mass-loss rate, we decreased it in a trial-and-error manner, while keeping all other input parameters constant. We found that a mass-loss rate of 3.9 $M_\oplus$ Gyr^{-1} resulted after one orbit in a reasonable transit depth compared to that observed on average. However the tail had not reached a steady state. Evolving it for two more orbits allowed it to reach a quasi-steady state[3], resulting in a significantly larger transit cross-section, producing deeper transits, as shown in Fig. 4.3. The light curve after one orbit matches the pre-ingress forward scattering peak, depth and width reasonably well but like the tails presented in Chapter 3, it over-estimates the forward scattering at egress. The light curves after evolving over a timescale of three orbits are deeper and better reproduce the extended egress. If the tail is allowed to evolve for several orbits until it reaches a steady state, a mass-loss rate of 3 $M_\oplus$ Gyr^{-1} (down from 7 $M_\oplus$ Gyr^{-1} in the non-self-shielding case) reproduces a transit depth comparable to the average long-cadence light curve of Kepler-1520 b.

The reduced sublimation rate allows particles to survive for more than one orbit, which violates the observed lack of correlation between consecutive transit depths (van Werkhoven et al. 2014). To estimate the magnitude of the correlation that would be produced, we stopped ejecting new particles into this tail after one orbit and let the tail evolve for two more orbits. The tail had completely sublimated by the time of the third transit, however, there was still a significant tail present at the time of the second transit, as shown in Fig. 4.4. The tail from these persisting particles is relatively optically thin with a maximum optical depth of $\tau = 0.57$ and a mean optical depth of 0.10. The transit light curve that this tail produces is shown in Fig. 4.4 and has a transit depth of approximately 0.3% and reproduces the extended egress better than the previously presented tails because the particles have had more time to be distributed along the tail.

4.3.3 Reduction of the intrinsic sublimation rate

To determine whether it is possible for a self-shielding tail produced by a mass-loss rate of 3.9 $M_\oplus$ Gyr^{-1} to result in uncorrelated consecutive transit depths as should be the case for Kepler-1520 b, we simulated a tail with the same input parameters

[3]The reduced sublimation rate from self-shielding prevents the particles being lost at the same rate as they are being added, however the tail morphology is constant after two orbits. We reduced the number of particles by a factor of 10 to allow us to run a simulation of continual mass-loss for many orbits and found that it reached an approximate steady state after 10 orbits.

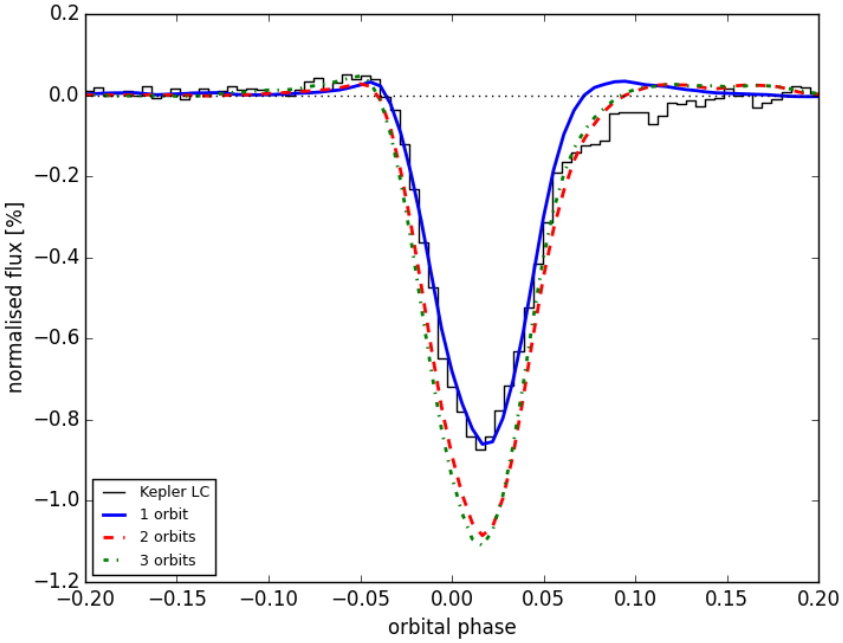

Figure 4.3: Light curves produced by a mass-loss rate of 3.9 $M_{\oplus}$ Gyr^{-1} after one (blue solid), two (red dashed) and three (green dashed-dotted) orbits of continuous mass-loss for Kepler-1520 b.

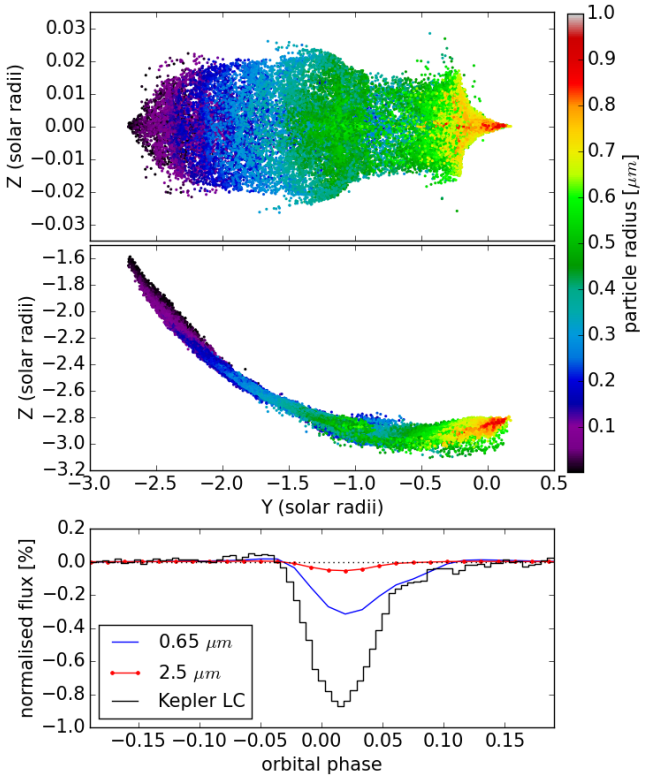

Figure 4.4: Same as a column in Fig. 4.2 after one orbit of losing mass at a rate of 3.9 $M_\oplus$ Gyr^{-1} and a second orbit without losing any mass for Kepler-1520 b.

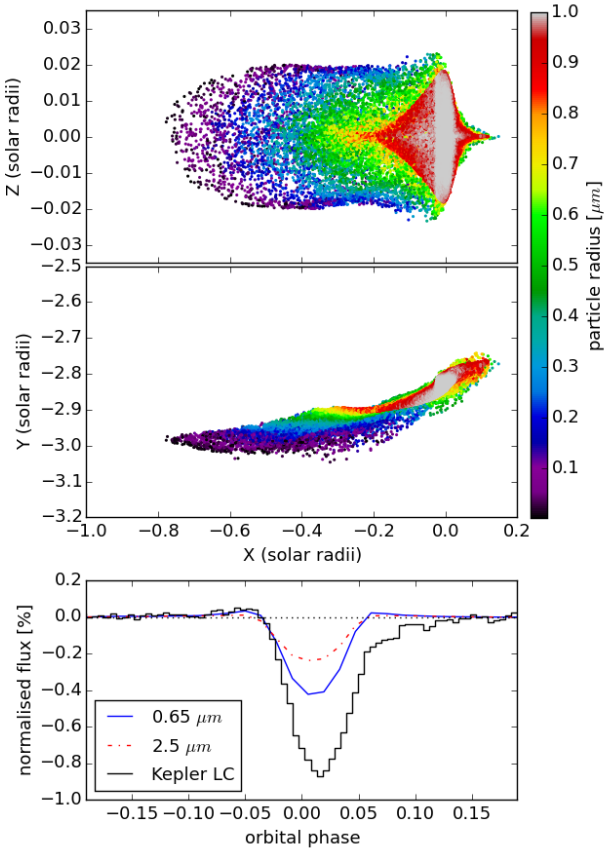

Figure 4.5: Same as a column in Fig. 4.2 except with a mass-loss rate of 3.9 $M_\oplus$ Gyr^{-1} and an intrinsic sublimation rate increased by a factor of three.

as the one presented in Section 4.3.2 but increased the intrinsic sublimation rate by a factor of three. We continuously ejected particles for the first orbit, then stopped ejecting particles, and let the tail continue to evolve. With this increased sublimation rate, all of the particles had sublimated after 1.8 orbits, which may result in uncorrelated consecutive transit depths if the particles for the next orbit are ejected in the last 20% of its orbit. This tail and its light curve are shown in Fig. 4.5. The shorter length of this tail reduces the transit depth and duration.

4.3.4 Short-time scale outbursts

Shielded particles receive a reduced stellar flux which causes them to sublimate and drift away from the planet at a reduced rate. This means that a significant tail

can form, even if all of the particles are ejected on a timescale that is much shorter than the orbital period. To demonstrate this concept in the framework of Kepler-1520 b, we simulated a tail with a high initial mass-loss rate of 780 $M_{\oplus}$ Gyr^{-1} for only 1% of its first orbit and allowed it to evolve until three orbits had elapsed. This is equivalent to the mass-loss rate found in Chapter 3 that was needed for a non-self-shielding tail to match the average transit depth of Kepler-1520 b. To highlight the difference caused by accounting for the self-shielding, we also simulated a tail that neglected self-shielding but used almost identical input parameters. The only parameter that we changed was the sublimation rate, which we reduced by a factor of three. This was necessary to allow the particles in the non-self-shielding case to survive for three orbits to be comparable to the longer surviving particles in the self-shielding case. The simulated tails for both cases at the times of 0.6, 1.2, 1.8, 2.4 and 3.0 orbital periods are shown in Figs. 4.6 and 4.7.

In the non self-shielding case, all of the particles immediately experience the full radiation pressure and independently follow their rosette-like trajectories in a reference frame co-rotating with the planet (e.g. Rappaport et al. 2014; van Lieshout et al. 2014). If a single particle were tracked over these three orbits, it would pass through each of the arcs shown in the top left panel of Fig. 4.7. Without self-shielding to reduce the radiation pressure, the particles drift approximately half an orbital circumference away from the planet. Due to the particles moving far away from the planet, the timing of the transit varies.

In the self-shielding case, the tail initially has a high density and optical depth. The average optical depth for 0.6, 1.2, 1.8, 2.4 and 3.0 orbits are $\tau = 3.8$, 1.2, 0.60, 0.76 and 0.28, respectively. This significantly changes the particle dynamics and the resulting tail morphology and transit light curve. It shows that the particle sublimation rate can be affected enough to allow a significant tail to be present three orbits after ejecting an optically thick cloud of particles. If the mass-loss from the planet did occur in bursts shorter than an orbital period, this could have an implication on the total mass-loss rate from the planet, because mass-loss is generally assumed to be continuous (e.g. Perez-Becker & Chiang 2013). However, such a scenario could not be responsible for the case of Kepler-1520 b because it would lead to a correlation between consecutive transits which is not observed (van Werkhoven et al. 2014).

Taking an average of the light curves at the times of 0.6, 1.2, 1.8, 2.4 and 3.0 orbits significantly reduces forward scattering at egress, alleviating the issue with some of our other models. This suggests that average light curves may be best reproduced by averaging the light curves produced by different tail morphologies, such as those shown in Fig. 4.6, which cancel out the forward scattering peak that would otherwise occur at egress.

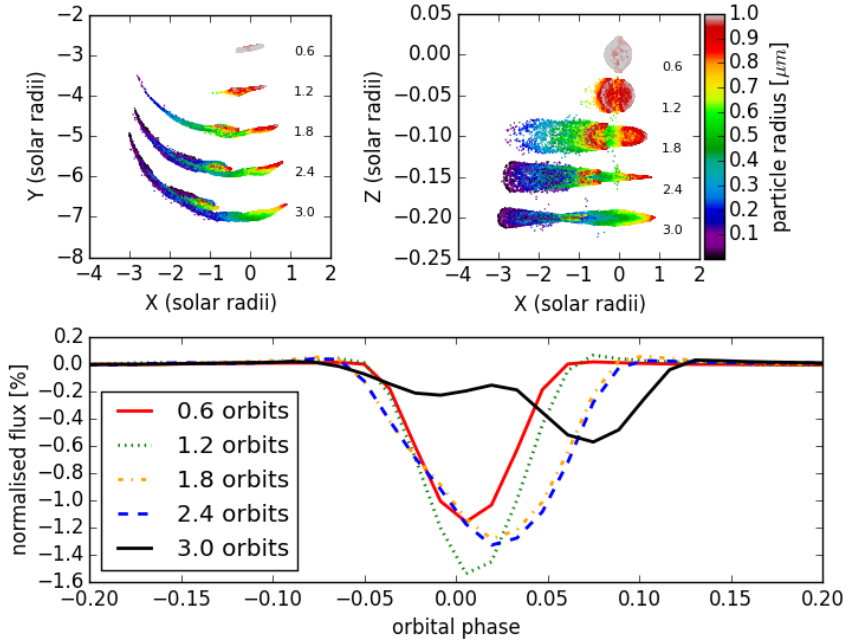

Figure 4.6: Series of snapshots of an optically thick tail that was produced by a large initial outburst with mass-loss rate 780 $M_\oplus$ Gyr^{-1} that only lasted for 1% of the first orbit. This mass-loss rate is equivalent to a mass-loss rate of 7.8 $M_\oplus$ Gyr^{-1} that lasts for the entire orbit.

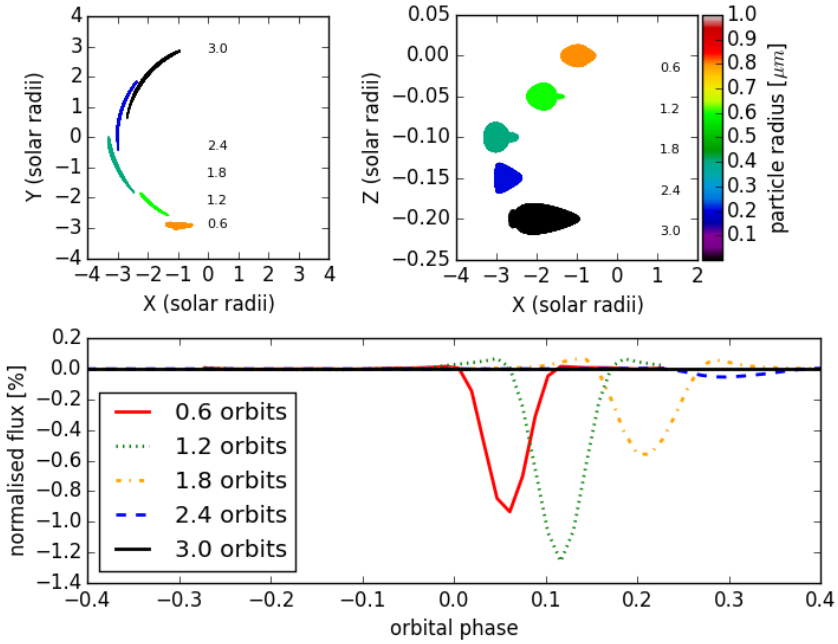

Figure 4.7: Like Fig. 4.6 except in this case the tail's self-shielding was neglected. The sublimation rate was also decreased by a factor of three to allow the non-shielded particles to survive for three orbits.

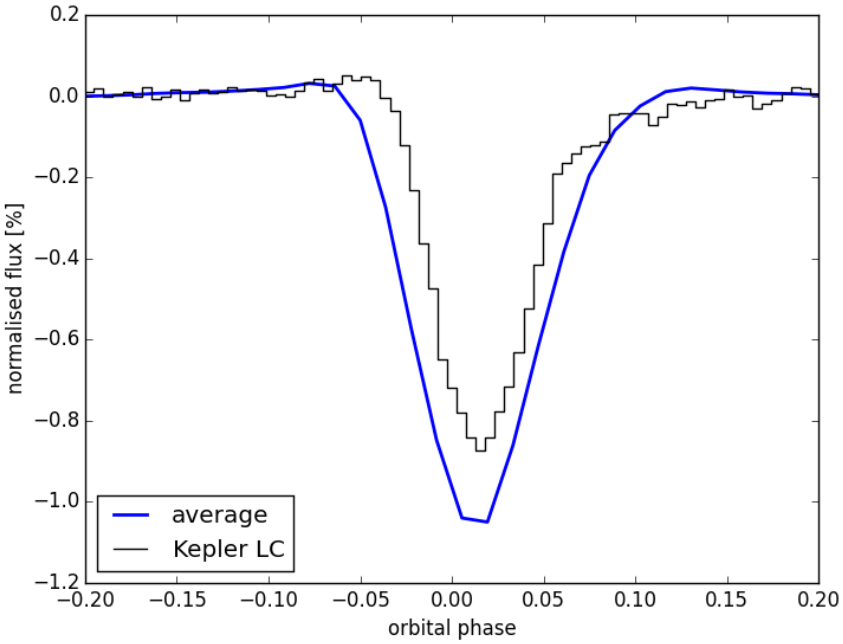

Figure 4.8: The average of the light curves shown in Fig. 4.6 (blue) compared the average Kepler long cadence light curve of Kepler-1520 b (black steps). The excessive forward scattering at egress that is present in some of our other individual light curves is not present in this average.

4.3.5 Highly optically thick regime

As shown in Fig. 4.2, a high mass-loss rate makes the tail form much slower because the shielded particles move away from the planet more slowly as a result of the reduced radiation pressure. However, if high mass-loss rate tails are allowed to evolve for more than one orbit, a significant tail can form, as shown in Figs. 4.9 and 4.10 for mass-loss rates of 10 and 100 $M_{\oplus}Gyr^{-1}$, respectively. The first row shows a non-self-shielding tail that is in a steady state after one orbit. The middle three rows show the evolving tail after continuously losing mass for three orbits, and the bottom row shows the simulated transit light curves at these different times.

The 100 $M_{\oplus}Gyr^{-1}$ tail was challenging to model because its high density required an optical depth grid that had a higher resolution than what we were able to use due to computational limitations. This prevented us from modeling the optically thin surface layer that should be present in an optically thick tail. However, we approximated it by setting the optical depth of the cells along the surface of the tail facing the star to zero, allowing all of the particles within these surface layer cells to experience the full radiation pressure. This is an upper limit because in reality only particles within part of the surface layer cells will experience the full radiation pressure. The number of particles in the 0.1 and 1 $M_{\oplus}Gyr^{-1}$ cases in Fig. 4.2 stayed at a steady value after one orbit. However, after running for the maximum time of three orbits set by computational limitations, the 10 and 100 $M_{\oplus}Gyr^{-1}$ cases did not reach a steady state in particle numbers. Despite this, the shape of the tail did not significantly change from the second to the third orbit, indicating that it had reached a quasi-steady state.

The slow tail formation occurs because the particles in the exposed surface layer sublimate and experience a stronger radiation pressure, which peaks for particle sizes around 0.1 μm (e.g. van Lieshout et al. 2014). This stronger radiation pressure pushes the surface layer particles further into the tail, which significantly reduces the radiation pressure that they experience.

This slow tail formation rate implies that very high mass-loss rates would produce correlated increasing transit depths, which has not been observed in any of the currently known disintegrating rocky exoplanets. However, it is likely that TESS will discover more of these objects and if some exhibit correlated transits that increase in depth, it may indicate an intermittent high mass-loss rate from the planet.

4.4 Conclusions

We have shown that self-shielding of dust tails from disintegrating rocky exoplanets can affect the tail morphology. In particular, we show that a self-shielding dust tail can produce a reasonable match to the Kepler average long cadence light curve

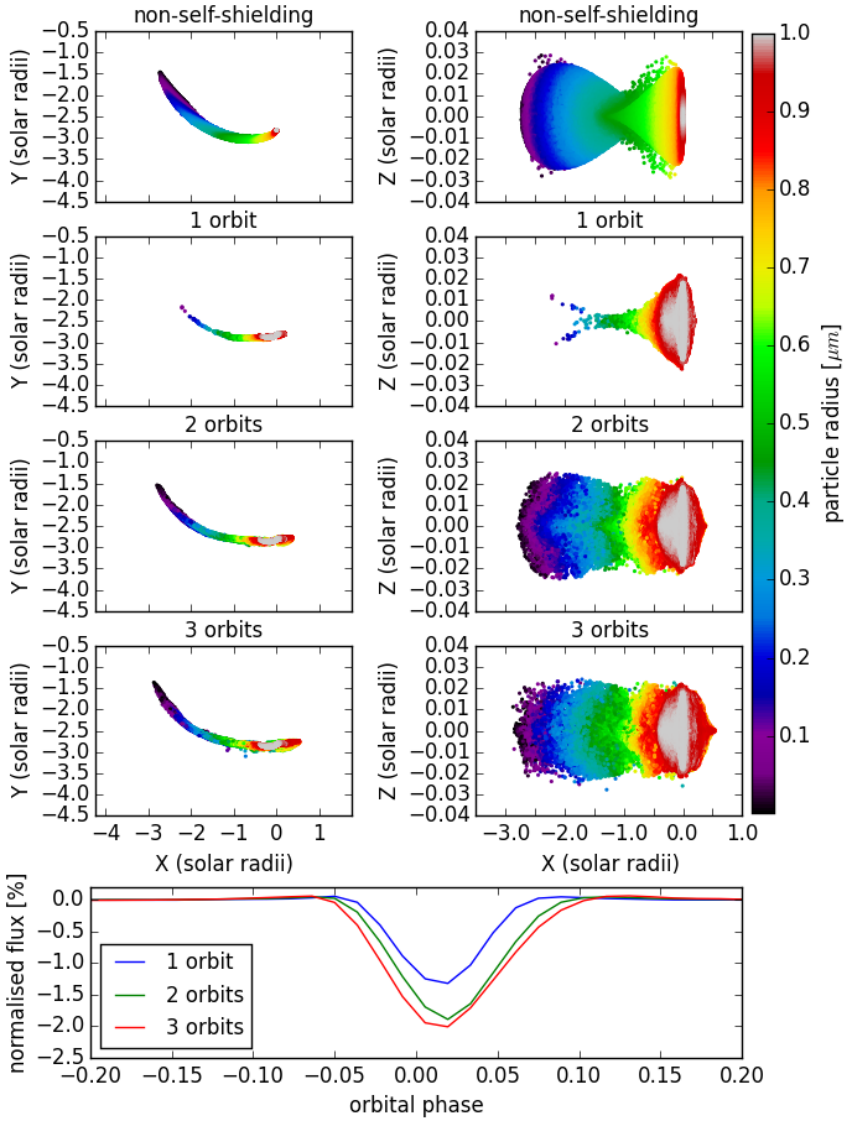

Figure 4.9: Evolution of a highly self-shielding tail produced by a planet mass-loss rate of 10 $M_\oplus$ Gyr^{-1}. Left: View of the tail from above the orbital plane. Right: View of the tail from the orbital plane. The first row shows a non-self-shielding tail that is in a steady state after one orbital period. The three middle rows show a self-shielding tail of mass-loss rate 10 $M_\oplus$ Gyr^{-1} after one, two and three orbits. The last row shows the transit light curves produced by the self-shielding tail after evolving for one, two and three orbits.

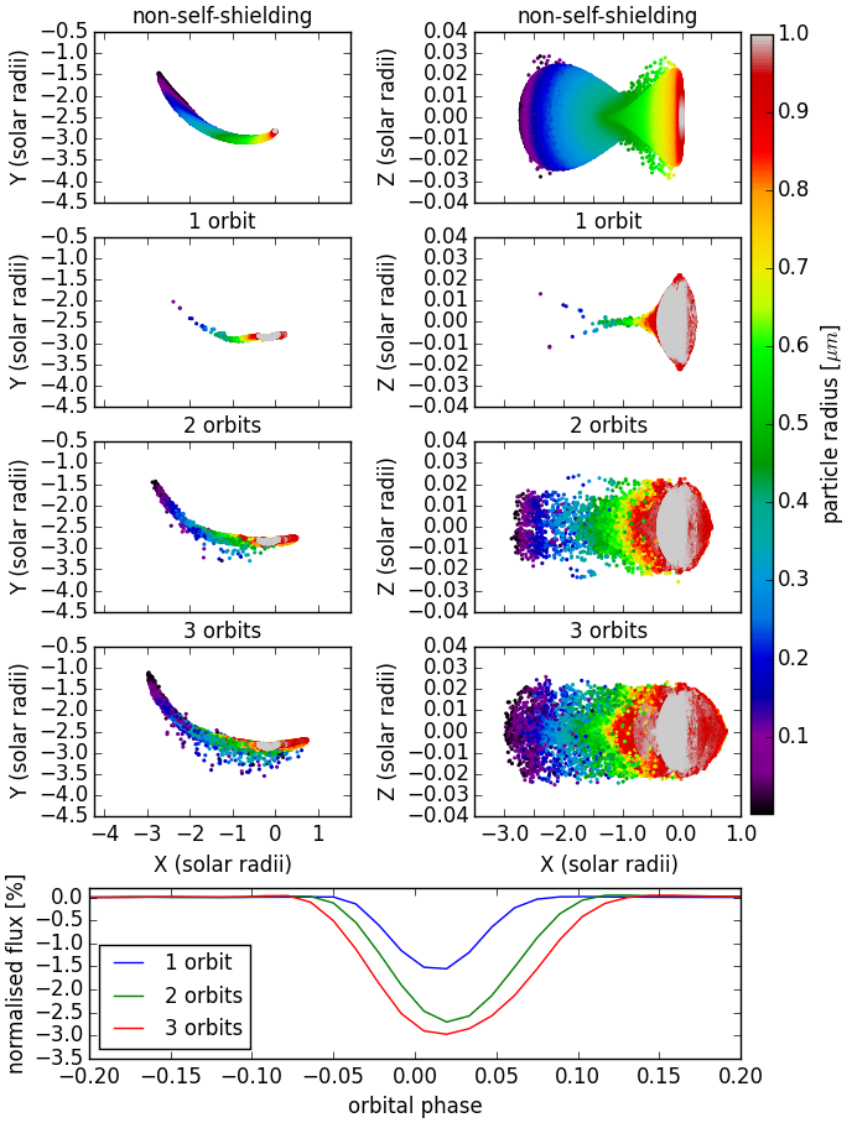

Figure 4.10: Same as for Fig. 4.9 except for using a mass-loss rate of 100 $M_\oplus$ Gyr^{-1}.

of Kepler-1520 b with a mass-loss rate of $3 - 3.9$ $M_\oplus$ Gyr^{-1} which is lower than the rate that was required for a non-self-shielding tail in Chapter 3. However, they provide so much self-shielding that particles can survive for more than one orbital period, leading to correlations between consecutive transit depths which are not observed (van Werkhoven et al. 2014). Lower mass-loss rates with a more volatile material (with a faster intrinsic sublimation rate) can alleviate this issue, however these tails produce shallow transit depths due to their reduced length and transit cross-section.

We demonstrate that a tail can form with a mass-loss time scale that is much shorter than an orbital period. This may have implications for calculated mass-loss rates, which are usually assumed to occur over an orbital period (e.g. Perez-Becker & Chiang 2013). We also show that tails with mass-loss rates $\gtrsim$10 $M_\oplus$ Gyr^{-1} take a significantly longer time to form due to the strong self-shielding reducing the radiation pressure and drift rate away from the planet. This scenario would produce correlated increasing transit depths, which may provide a way to identify tails that were produced by high mass-loss rates in the era of TESS.

4.5 Future outlook

TESS is expected to discover several disintegrating rocky exoplanets around brighter stars, making detailed observational characterisation possible. The interpretation of these observations will depend critically on the accuracy of the dust-tail models that are used.

Gas is expected to be present in dust tails because it will be produced by the sublimation of dust particles and the planet's mass-loss mechanism which likely involves a gaseous outflow (Perez-Becker & Chiang 2013). Therefore, future models should account for gas pressure affecting the particle dynamics. This modeling effort will be significantly aided by observational constraints on gas density.

Since the dust particles likely condense in a gaseous outflow from the planet (Perez-Becker & Chiang 2013), a better understanding of the density of gas may enable the initial dust-grain size distribution to be better understood. This distribution may affect the tail's density profile so it should also be accounted for in future models.

Acknowledgements

A. R. R.-H. is grateful to the Planetary and Exoplanetary Science (PEPSci) programme of the Netherlands Organisation for Scientific Research (NWO) for support. I. A. G. S. acknowledges support from an NWO VICI grant (639.043.107).

Bibliography

Alonso, R., Rappaport, S., Deeg, H. J., & Palle, E. 2016, A&A, 589, L6

Bochinski, J. J., Haswell, C. A., Marsh, T. R., Dhillon, V. S., & Littlefair, S. P. 2015, ApJ, 800, L21

Bourrier, V., Lecavelier des Etangs, A., & Vidal-Madjar, A. 2014, A&A, 565, A105

Brogi, M., Keller, C. U., de Juan Ovelar, M., et al. 2012, A&A, 545, L5

Budaj, J. 2013, A&A, 557, A72

Burns, J. A., Lamy, P. L., & Soter, S. 1979, Icarus, 40, 1

Croll, B., Rappaport, S., DeVore, J., et al. 2014, ApJ, 786, 100

Koike, C., Kaito, C., Yamamoto, T., et al. 1995, Icarus, 114, 203

Min, M., Dullemond, C. P., Dominik, C., de Koter, A., & Hovenier, J. W. 2009, A&A, 497, 155

Min, M., Hovenier, J. W., & de Koter, A. 2005, A&A, 432, 909

Murgas, F. 2013, PhD thesis, Departamento de astrofisica, unisersidad de La Laguna

Perez-Becker, D. & Chiang, E. 2013, MNRAS, 433, 2294

Rappaport, S., Barclay, T., DeVore, J., et al. 2014, ApJ, 784, 40

Rappaport, S., Levine, A., Chiang, E., et al. 2012, ApJ, 752, 1

Sanchis-Ojeda, R., Rappaport, S., Pallè, E., et al. 2015, ApJ, 812, 112

van Lieshout, R., Min, M., & Dominik, C. 2014, A&A, 572, A76

van Lieshout, R., Min, M., Dominik, C., et al. 2016, A&A, 596, A32

van Werkhoven, T. I. M., Brogi, M., Snellen, I. A. G., & Keller, C. U. 2014, A&A, 561, A3

Vanderburg, A., Johnson, J. A., Rappaport, S., et al. 2015, Nature, 526, 546